International Journal of
Molecular Sciences

MDPI

Article

Selenium-Thioredoxin Axis Contributes to Ferroptosis Resistance in Pancreatic Cancer Cells

Arslan Amer, Micah Idowu, Aqsa Ahsan, Alyssa Abbas, Tahiyat Alothaim † and Xiaohu Tang *

Department of Biological Sciences, Michigan Technological University, Houghton, MI 49931, USA; aamer@mtu.edu (A.A.); aahsan@mtu.edu (A.A.); taalotha@mtu.edu (T.A.)

* Correspondence: xiaohut@mtu.edu; Tel.: +1-906-487-3068

† Current address: Department of Biology, College of Science, Qassim University, Buraydah 51452, Al-Qassim, Saudi Arabia.

Abstract

Pancreatic ductal adenocarcinoma (PDAC) shows substantial heterogeneity in cysteine dependence and ferroptosis sensitivity. We identify two PDAC subtypes distinguished by EMT status: mesenchymal-like cells are highly cysteine-dependent and rapidly undergo ferroptosis upon cystine deprivation or system xc^- inhibition, whereas epithelial-type cells are ferroptosis-resistant. Selenium supplementation protects cells from erastin-induced ferroptosis, and this protection persists even when intracellular glutathione (GSH) is depleted, supporting an additional GPX4-independent protective mechanism. Sepp1 knockdown does not alter sensitivity, indicating that selenium's protective effect is independent of Sepp1. Instead, epithelial-type cells rely on both cytosolic and mitochondrial thioredoxin reductases (TrxR1 and TrxR2) to maintain ferroptosis resistance. Chemical inhibition of thioredoxin reductases abolishes selenium-mediated protection and sensitizes epithelial cells to ferroptosis inducers, while dual genetic suppression of TrxR1 and TrxR2 similarly restores ferroptosis sensitivity. These findings uncover a selenium–thioredoxin redox axis that functions independently of GPX4 and contributes ferroptosis resistance in epithelial-type PDAC cells. Co-targeting cysteine metabolism and thioredoxin reductases may therefore represent a rational strategy to overcome ferroptosis resistance in some PDAC subtypes.

Keywords: ferroptosis; PDAC; EMT; thioredoxin; selenium; resistance

1. Introduction

Pancreatic ductal adenocarcinoma (PDAC) remains one of the deadliest malignancies, with a five-year survival rate below 12% despite major advances in molecular characterization and treatment strategies [1–4]. PDAC is defined by profound metabolic rewiring driven in part by oncogenic KRAS, which is mutated in more than 90% of PDAC cases, promoting elevated reactive oxygen species (ROS), altered redox homeostasis, and increased reliance on antioxidant pathways [5–10]. Among these vulnerabilities, ferroptosis, an iron-dependent form of cell death driven by uncontrolled lipid peroxidation, has emerged as a promising therapeutic avenue for PDAC and other solid tumors [11]. Recent reviews highlight the therapeutic potential of ferroptosis induction through system xc^- inhibition, cysteine depletion, nanoparticle-based delivery of ferroptosis inducers, and metabolic combination therapies [12–16].

Cysteine metabolism is central to maintaining redox homeostasis, serving as a precursor for glutathione (GSH) synthesis and other thiol-based antioxidants [14,17–19]. PDAC

Check for updates

Academic Editor: Dongki Yang

Received: 1 December 2025
Revised: 20 February 2026
Accepted: 20 February 2026
Published: 23 February 2026

Copyright: © 2026 by the authors. Licensee MDPI, Basel, Switzerland. This article is an open access article distributed under the terms and conditions of the Creative Commons Attribution (CC BY) license.

cells exhibit strong cystine/cysteine dependence, and inhibition of system xc^- or cysteine depletion induces rapid ferroptosis in a subset of PDAC models [20–23]. However, ferroptosis sensitivity is highly heterogeneous, and many tumor cells utilize parallel antioxidant systems, including FSP1, peroxiredoxins, and the thioredoxin (Trx) pathway, to limit lipid peroxidation independently of GPX4 [24–26].

Emerging evidence also links epithelial–mesenchymal transition (EMT) programs to ferroptosis sensitivity. EMT alters lipid composition, ROS [27,28], and metabolic wiring, and cancers including PDAC show mesenchymal-like cells can be more ferroptosis-prone under cysteine stress [8,19,27–32]. Transcriptional profiling has classified PDAC into epithelial and mesenchymal subtypes with distinct vulnerabilities. These observations raise the possibility that EMT state may serve as a functional determinant of ferroptosis sensitivity, despite the underlying mechanisms remaining incompletely understood [28].

Selenium metabolism adds another layer of ferroptosis regulation [33]. Through selenocysteine incorporation, selenium supports antioxidant selenoproteins that suppress ferroptosis [34–36]. Particularly, selenium availability has been observed to inversely correlate with cancer progression, suggesting a protective role in some context [36,37]. GPX4, one of twenty-five human selenoproteins, reduces lipid hydroperoxides using glutathione (GSH) as a cofactor and is a key ferroptosis regulator [34,38]. Inhibition of GPX4 function by either blocking cysteine uptake (erastin) or its direct inhibitor (RSL-3) triggers ferroptosis [38,39].

The plasma selenium transporter Sepp1 delivers selenium to peripheral tissues and influences redox buffering, metabolic remodeling, and clinical outcome in cancers [37,40]. Recent studies have revealed that selenium does not uniformly support GPX4, but instead is differentially partitioned among selenoproteins, including PRDX6 and TrxR enzymes, in ways that can alter ferroptosis sensitivity independent of GPX4 [37,41,42]. These insights highlight the importance of understanding selenium-driven, GPX4-independent antioxidant mechanisms in PDAC. However, the specific contribution of Sepp1 or selenium to PDAC ferroptosis sensitivity remains unclear.

The thioredoxin (Trx) system, comprising thioredoxin (Trx), thioredoxin reductases (TrxR1/TrxR2), and NADPH, is a major parallel antioxidant pathway that detoxifies peroxides independently of the GSH–GPX4 axis [37,43,44]. Both TrxR1 and TrxR2 are frequently elevated in PDAC and other cancers, supporting survival under oxidative stress [44–48]. Being a selenite reducing enzyme as well as a selenol-containing enzyme, TrxR plays a central role in selenium pathophysiology [46,49]. Growing evidence now links thioredoxin reductases to GPX4-independent ferroptosis resistance, and inhibition of TrxR1 sensitizes diverse cancer cells to system xc^- blockade, glutathione depletion, or cysteine stress in some tumor cells [44,49–51].

Here, we investigate how cysteine dependence, selenium utilization, and the thioredoxin system collectively shape ferroptosis sensitivity across PDAC subtypes. We identify two phenotypically distinct PDAC groups differing in ferroptosis susceptibility, refine the contribution of selenium beyond GPX4, and uncover a previously underappreciated role for the thioredoxin system as a GPX4-independent ferroptosis-defense axis. Together, these findings reveal a targetable metabolic–redox interaction in PDAC and motivate deeper mechanistic and therapeutic exploration.

2. Results

2.1. Pancreatic Cancer Cells Exhibit Differential Cysteine-Dependence

Ferroptosis inducers that block cysteine uptake (erastin) or directly inhibit GPX4 (RSL-3) can eliminate many different types of cancer cells effectively [20,21,52]. To evaluate ferroptosis sensitivity in pancreatic cancer, we examined the response of six PDAC cell lines

to erastin treatment. PANC-1 and MIAPaCa-2 cells exhibited marked sensitivity, whereas the epithelial primary tumor lines CAPAN-2 and BXPC-3 and epithelial metastatic lines CFPAC-1 and ASPC-1 were highly resistant (Figures 1A and S1A). Cell death occurred rapidly (within 14–18 h), accompanied by characteristic membrane rupture (Figure S1B). Consistent with loss of membrane integrity, elevated extracellular protease activity was detected in the culture media of sensitive cells (Figure 1B).

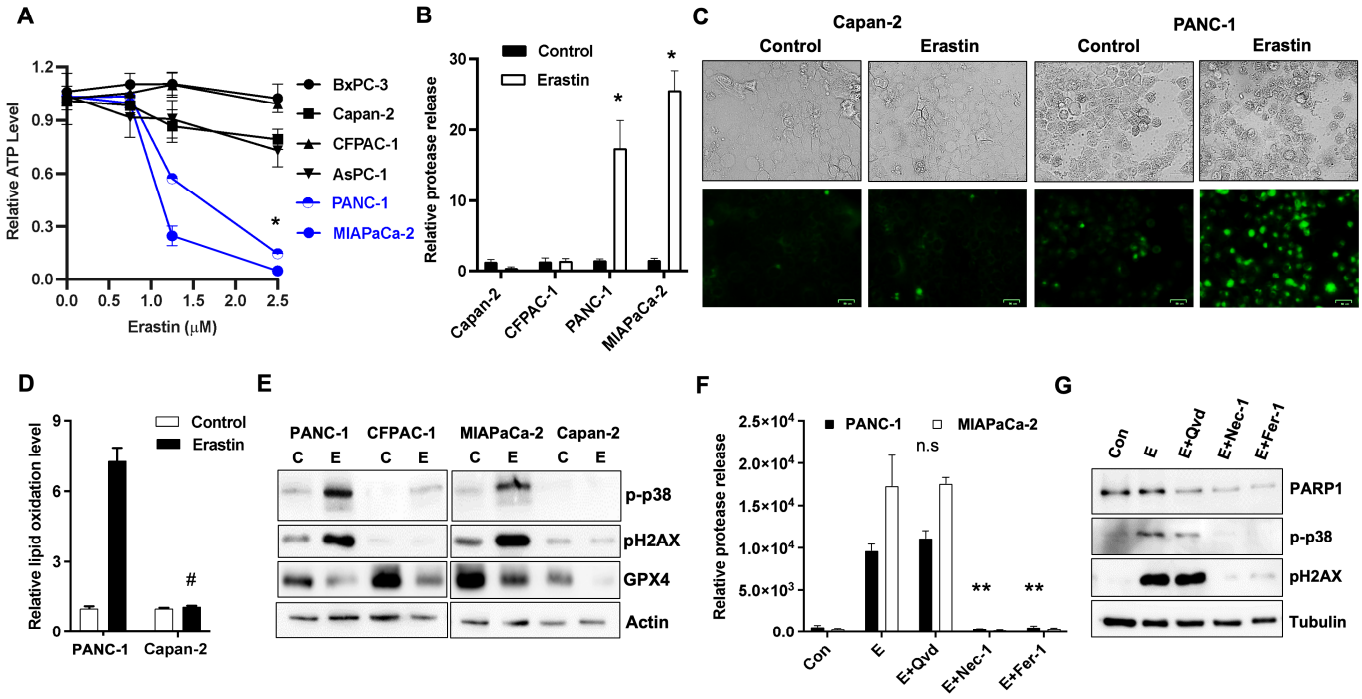


Figure 1. Ferroptosis inducers trigger selective cell death in pancreatic tumor cells. (**A**). Relative viability of pancreatic tumor cell lines following 48 h of erastin treatment at the indicated concentrations, measured by the CellTiter-Glo® ATP assay (n = 3; * p < 0.002). (**B**). Cytotoxicity in Capan-2, CFPAC-1, PANC-1, and MIAPaCa-2 cells after control or 2.5 μM erastin treatment for 18 h, assessed by protease-release CytoTox-Fluor assay (n = 3, * p < 0.005). (**C**). Lipid peroxidation in Capan-2 and PANC-1 cells visualized using the Image-iT™ Lipid Peroxidation Assay under control or 2.5 μM erastin treatment for 16 h. Lower panels show the fluorescence signal; upper panels show corresponding bright-field morphology (Scale bar: 30 μm). (**D**). Quantification of lipid peroxidation in the indicated cell lines treated as in (**C**) (n = 3, # p < 0.003). (**E**). Immunoblot analysis of phosphorylated p38, phosphorylated H2AX, and GPX4 protein expression in the indicated cells treated with control or erastin for 16 h. β-Actin serves as a loading control. (**F**). Cytotoxicity of PANC-1 and MIAPaCa-2 cells after treatment with control, erastin, or erastin in combination with Q-Vad (Qvd, 20 μM), Necrostatin-1 (Nec-1, 10 μM), or Ferrostatin-1 (Fer-1, 5 μM) for 18 h (n = 3, ** p < 0.001; n.s., not significant). (**G**). Immunoblot analysis of cell death and stress markers in MIAPaCa-2 cells treated as in (**F**). α-Tubulin serves as a loading control.

To determine whether ferroptosis was driving this differential response, we assessed lipid peroxidation, a hallmark and trigger of ferroptosis. Erastin-induced robust lipid peroxidation exclusively in the eratin-sensitive PANC-1 cells, whereas erastin-resistant Capan-2 cells showed minimal or undetectable lipid peroxidation (Figure 1C,D). In agreement with these phenotypes, Western blot analysis revealed activation of stress-associated death signaling (p-p38) and DNA damage (p-H2AX) only in erastin-sensitive cells (Figure 1E). Similar patterns were observed with RSL3, a GPX4 inhibitor, which likewise produced clear sensitivity differences across PDAC lines (Figure S1C). The erastin-induced cell death and death markers were significantly prevented by the non-specific necrosis inhibitor Necrostatin-1 and the ferroptosis inhibitor Ferrostatin-1, but not by the broad-spectrum

caspase inhibitor Q-Vad (Figures 1F,G and S1D). Although the phosphorylation of p38 and γH2AX are not specific markers of ferroptosis, their selective induction in erastin-sensitive cells and suppression by Ferrostatin-1 support their use here as contextual indicators of ferroptosis. Together with robust lipid peroxidation and caspase-independent, Ferrostatin-1-reversible cell death, these data support ferroptosis as the predominant mode of death in the erastin-sensitive cells.

Together, these findings indicate potential inter-tumoral heterogeneity in cysteine dependence and ferroptosis susceptibility among PDAC. This prompted us to define the molecular determinants of this variability and to test whether distinct cellular programs underlie the observed ferroptosis phenotypes.

2.2. Cysteine Dependence Is Associated with the EMT Status of Pancreatic Cancer Cells

Two ferroptosis inducers, erastin and RSL3, were originally identified for their ability to selectively kill oncogenic RAS-mutant cells in vitro [39,53]. Because KRAS mutations are a hallmark of PDAC, we first assessed whether KRAS status influenced ferroptosis sensitivity. Five of six PDAC cell lines harbored oncogenic KRAS mutations (Figure S2A), yet mutation status did not correlate with erastin sensitivity, indicating that factors beyond RAS activation govern cysteine dependence. In contrast, Smad4, an essential mediator of TGF-β signaling and EMT [54,55], was mutated or lost in four erastin-resistant lines but retained in both erastin-sensitive lines (Figure S2A). This pattern suggested a possible association between Smad4 status and ferroptosis sensitivity. However, forced Smad4 expression in resistant cells induced only minor changes in EMT marker levels (Figure S2C) and failed to alter erastin sensitivity (Figure S2B), indicating that Smad4 loss alone does not drive ferroptosis resistance in PDAC.

Previous studies have linked phenotypic cysteine dependence to EMT status in breast cancer [19,27]. To determine whether EMT status similarly correlates ferroptosis sensitivity in PDAC, we performed unsupervised clustering and gene set enrichment analysis (GSEA) using the transcriptomic profiles (GSE21456) of all six PDAC cell lines used in this study. Cluster analysis grouped the cell lines into two distinct subgroups (Figure 2A), which aligned precisely with their erastin sensitivity (Figure 1A). The erastin-sensitive subgroup (PANC-1 and MIAPaCa-2) exhibited strong mesenchymal features, including elevated expression of Vimentin and ZEB1. SMAD9 also showed increased expression in this group, as identified through our unbiased clustering analysis. In contrast, the four erastin-resistant lines displayed epithelial characteristics, such as high E-cadherin, along with increased GATA3 and KLF5, which were also identified from this analysis despite not being classical epithelial markers. GSEA further confirmed enrichment of a mesenchymal gene signature, defined previously in breast cancer, in the erastin-sensitive PDAC subgroup (Figure 2B). Expression of representative EMT markers was validated at both the RNA (Figure 2C) and protein level (Figure 2E). Together, these results indicate that cysteine dependence and ferroptosis sensitivity in PDAC cells are closely associated with EMT status. Importantly, we interpret EMT markers here as phenotypic indicators of ferroptosis vulnerability rather than direct mechanistic drivers.

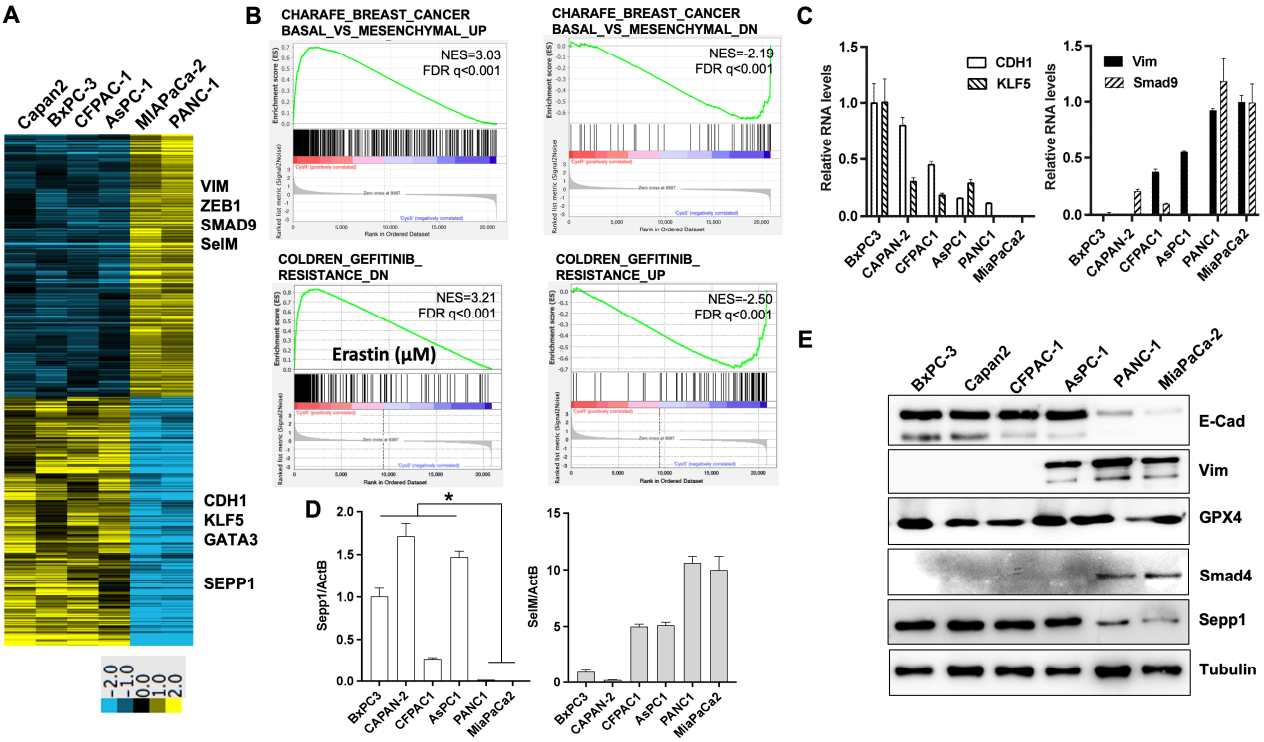


Figure 2. Phenotypic cysteine dependence correlates with the EMT status of pancreatic tumor cells. (**A**). Heatmap and hierarchical clustering of transcriptomic profiles from multiple pancreatic tumor cell lines. (**B**). GSEA showing that erastin-sensitive PDAC cells are enriched for EMT-associated gene signatures and a Gefitinib-resistance signature. (**C**). RT-qPCR analysis of epithelial- and mesenchymal-associated gene expression across the indicated cell lines. (**D**). RT-qPCR analysis of selenoprotein Sepp1 and SeIM in pancreatic tumor cells (n = 3, * p = 0.0006). (**E**). Immunoblot analysis of EMT markers, GPX4, and Sepp1 protein levels in indicated pancreatic tumor cells.

2.3. Selenium Protects Cells from Erastin-Induced Ferroptosis

From our transcriptomic analysis, two selenoproteins, Sepp1 and SelM, emerged as differentially expressed genes between PDAC subtypes (Figure 2A). These genes displayed nearly opposite expression patterns (Figure 2D). Given that Sepp1 functions as a selenium transport and storage protein, its reduced expression in erastin-sensitive cells could reflect limited selenium availability and altered selenoprotein metabolism in this subgroup.

To determine whether selenium influences ferroptosis sensitivity, we cotreated cells with sodium selenite and assessed their response to erastin. Selenite markedly protected erastin-sensitive PDAC cells from ferroptosis in a dose-dependent manner (Figures 3A,B and S3A,B). Consistent with this protective effect, selenite suppressed erastin-induced stress signaling (p-p38), DNA damage (p-H2AX), lipid peroxidation, and expression of death-associated genes (Figures 3C–E and S3D). In parallel, selenite increased GPX4 protein expression (Figure 3C). Selenite also rescued cells from RSL3-induced death, indicating a broader protective effect against ferroptosis (Figure S3C). Selenite had no observable effect on cell growth or viability in erastin-resistant cells, either treated alone or in combination with erastin.

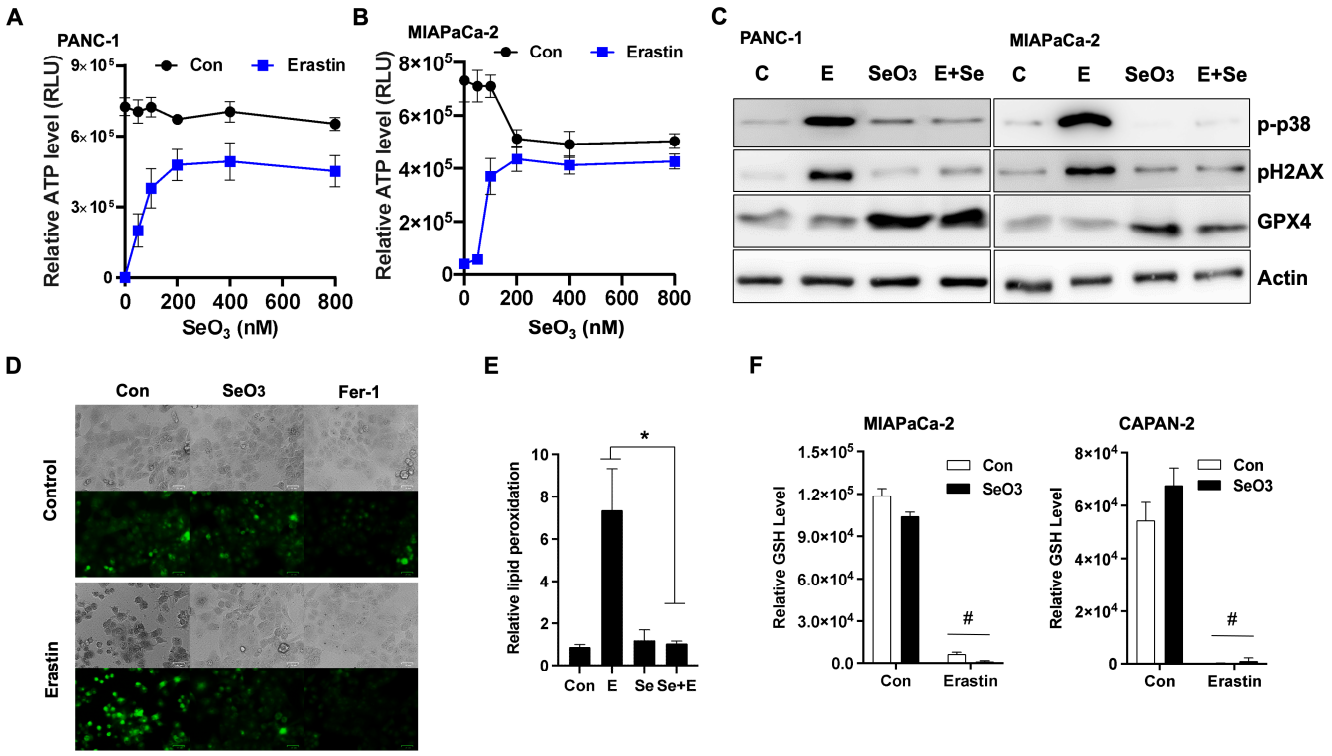


Figure 3. Selenite protects erastin-sensitive cells from ferroptosis. (**A**,**B**). Relative viability of PANC-1 and MIAPaCa-2 cells treated with control, erastin (2.5 μM), or erastin plus increasing concentrations of sodium selenite (SeO_3) for 48 h. (**C**). Immunoblot analysis of the indicated proteins in PANC-1 and MIAPaCa-2 cells treated with control (**C**), 2.5 μM erastin (**E**), or erastin plus 200 nM selenite for 16 h. (**D**). Lipid peroxidation in PANC-1 cells visualized using the Image-iT™ Lipid Peroxidation Assay after treatment with control, 2.5 μM erastin, erastin plus 200 nM selenite, or Ferrostatin-1 (Fer-1, 5 μM) for 48 h (Scale bar: 30 μm). (**E**). Quantification of lipid peroxidation in PANC-1 cells treated as (**D**) ($n = 3$, * $p = 0.03$). (**F**). Relative intracellular glutathione (GSH) levels in MIAPaCa-2 and CAPAN-2 cells treated as (**C**) ($n = 3$, # $p = 0.0169$).

However, despite increased GPX4 protein levels, intracellular glutathione (GSH) remained severely depleted under erastin plus selenite treatment (Figure 3F). Because GPX4 enzymatic activity strictly depends on the reduced GSH, these findings strongly suggest that GPX4 activity remains functionally impaired under these conditions despite elevated protein level. Although GPX4 activity and redox state were not directly assessed in this study, the depletion of intracellular GSH under these conditions suggests that selenium-mediated protection is largely independent of GPX4 activity.

2.4. Inhibition of the Thioredoxin System but Not Sepp1 Abolishes the Protective Effects of Selenium

Sepp1, a selenium transporter, was highly expressed in erastin-resistant PDAC cells but nearly absent in erastin-sensitive cells (Figure 2D,E). This inverse correlation suggested a potential role for Sepp1 in regulating cysteine dependence or oxidative stress in PDAC. Previous studies report that Sepp1 deficiency elevates ROS levels and promotes stem cell-like properties [56], suggesting the possibility that loss of Sepp1 in erastin-sensitive cells might impair selenium delivery and exacerbate ROS accumulation. To test whether Sepp1 contributes to ferroptosis resistance, we knocked down Sepp1 in erastin-resistant Capan-2 cells, confirming efficient depletion at the RNA expression level (Figure 4A). Unexpectedly, Sepp1 knockdown failed to increase erastin sensitivity, as cell viability and lipid peroxidation remained unchanged relative to controls (Figure 4B). These findings

indicate that Sepp1 is not a key determinant of ferroptosis resistance or cysteine dependence in PDAC cells.

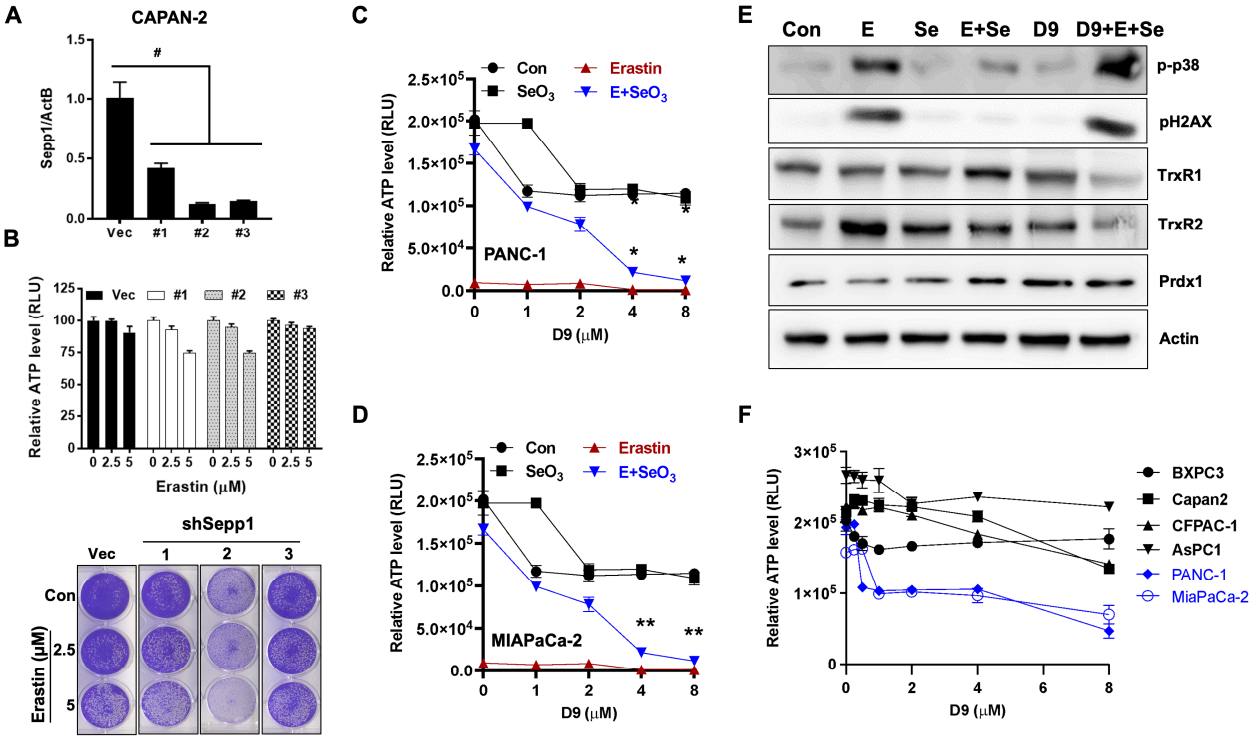


Figure 4. Inhibition of thioredoxin reductases abolishes the protective function of selenite against erastin-induced cell death. (**A**). RT-qPCR analysis of Sepp1 expression in Capan-2 vector control (Vec) and shSepp1 cells ($n = 3$, # $p < 0.05$). (**B**). Relative viability of Capan-2 Vec and shSepp1 cells, measured by CellTiter-Glo® assay and Crystal Violet staining, after control or erastin (2.5 or 5 μM) treatment for 96 h ($n = 3$, $p > 0.05$). (**C**,**D**). Relative cell viability of PANC-1 and MIAPaCa-2 cells treated with control, erastin (2.5 μM), selenite (200 nM), or erastin + selenite in combination with increasing concentrations of the thioredoxin reductase inhibitor D9 for 48 h ($n = 4$; * and ** $p < 0.001$). (**E**). Immunoblot analysis of the indicated proteins in PANC-1 cells treated with control (**C**), erastin (E; 2.5 μM), selenite (Se; 200 nM), E + Se, D9 (8 μM), or E + Se + D9 for 16 h. (**F**). Relative viability of pancreatic tumor cell lines treated with increasing concentrations of D9 for 48 h.

We next examined the thioredoxin (Trx) system, which includes the selenoproteins thioredoxin reductase 1 and 2 (TrxR1/TrxR2). The Trx system functions in parallel with the GPX4/GSH pathway to detoxify ROS [57], and selenium supplementation can enhance TrxR activity, suggesting that selenite may also protect cells through TrxR in addition to GPX4. To test this hypothesis, we used a thioredoxin reductase inhibitor D9. Increasing doses of D9 progressively abolished the protective effect of selenite against erastin-induced ferroptosis (Figure 4C,D). Immunoblotting confirmed that D9 restored erastin-induced stress signaling (p-p38) and DNA damage (p-H2AX), both of which were suppressed by selenite alone (Figure 4E). In addition, D9 cotreatment reduced TrxR1 and TrxR2 protein expression, confirming effective inhibition of the Trx system (Figure 4E). We also observed intrinsic variability in D9 sensitivity across PDAC cell lines. Mesenchymal/erastin-sensitive cells were markedly vulnerable to D9, whereas epithelial/erastin-resistant cells exhibited relative resistance (Figure 4F). These data suggest both pathways appear to act synergistically and erastin-resistant cells may rely on a more efficient thioredoxin system to escape cysteine depletion.

Collectively, these results demonstrate that selenium-dependent protection from ferroptosis requires an intact thioredoxin reduction system, not Sepp1.

2.5. Inhibition of the Thioredoxin System Sensitizes Epithelial-Type Pancreatic Tumor Cells to Erastin

As shown above, selenite-mediated protection from ferroptosis requires an intact thioredoxin (Trx) system, suggesting that this pathway may also confer intrinsic erastin resistance in epithelial-type PDAC cells. To test this hypothesis, we treated four epithelial-type/erastin-resistant PDAC cell lines with erastin in combination with the TrxR inhibitors. D9 markedly enhanced erastin-induced cell death in a dose-dependent manner, whereas either D9 or erastin alone produced minimal toxicity (Figures 5A,B and S4A,B). D9 cotreatment also restored erastin-induced death signaling (p-p38), DNA damage (p-H2AX), and expression of death-associated genes, all of which were suppressed when erastin was used alone in resistant cells (Figures 5C and S4C). Similarly, auranofin (Au), another TrxR inhibitor, produced similar sensitizing effects, confirming that TrxR blockade broadly enhances ferroptosis induction in epithelial-type PDAC cells (Figures 5D–F and S4D,E).

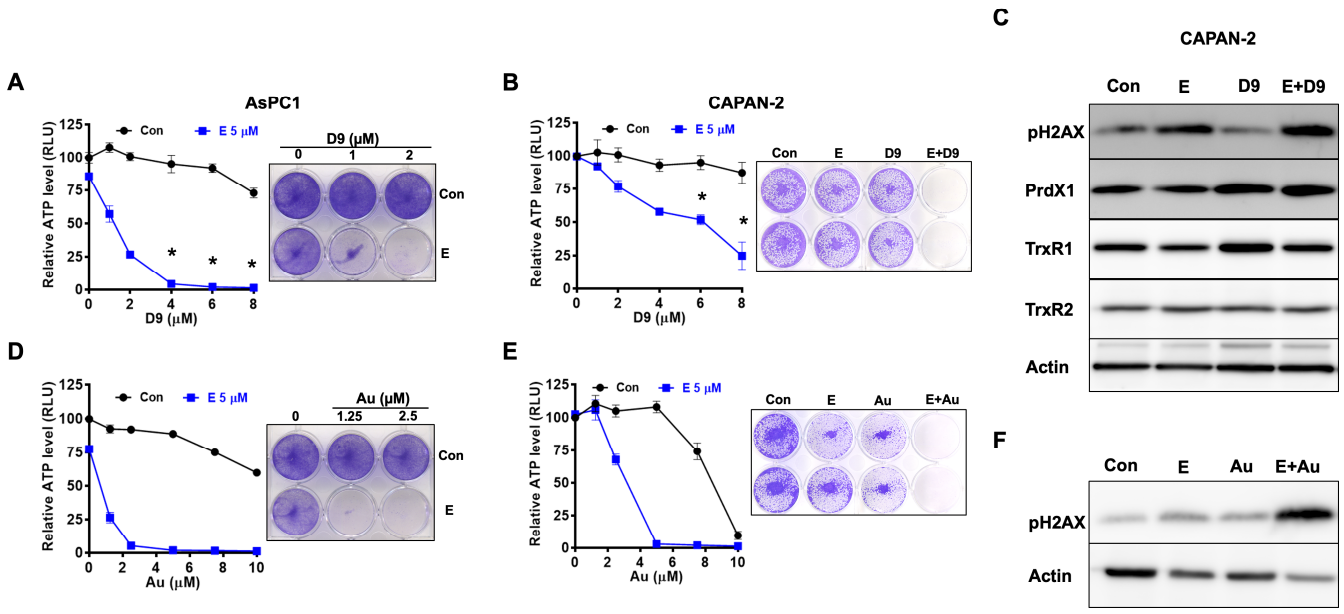


Figure 5. Thioredoxin reductase inhibition sensitizes erastin-resistant cells to ferroptotic death. (**A**,**B**). Relative viability of AsPC-1 and Capan-2 cells, measured by CellTiter-Glo® assay and Crystal Violet staining, after treatment with control, erastin (5 μM), or erastin plus increasing concentrations of the thioredoxin reductase inhibitor D9 for 72 h ($n = 3$, * $p < 0.001$). (**C**). Immunoblot analysis of the indicated proteins in Capan-2 cells treated with control, erastin (E, 5 μM), D9 (4 μM), or E + D9 for 36 h. (**D**,**E**). Relative viability of AsPC-1 and Capan-2 cells, measured by CellTiter-Glo® assay and Crystal Violet staining, after treatment with control, erastin (E, 5 μM), or erastin plus increasing concentrations of Auranofin (Au) for 72 h ($n = 3$, $p < 0.001$). (**F**). Immunoblot analysis of the indicated proteins in Capan-2 cells treated with control, erastin (5 μM), Auranofin (Au; 2.5 μM), or E + Au for 48 h.

Because the pharmacologic studies implicated TrxR activity in ferroptosis resistance, we next dissected the individual contributions of TrxR1 and TrxR2 enzymes, which localize to the cytosol and mitochondria, respectively. We used shRNA-mediated knockdown of each enzyme independently and confirmed efficient depletion in erastin-resistant cells (Figure 6B,D). Single knockdown of either TrxR1 or TrxR2 failed to restore erastin sensitivity, as cell viability and activation of death marker remained unchanged (Figure 6A–D). These results suggest functional redundancy between the cytosolic and mitochondrial thioredoxin pathways.

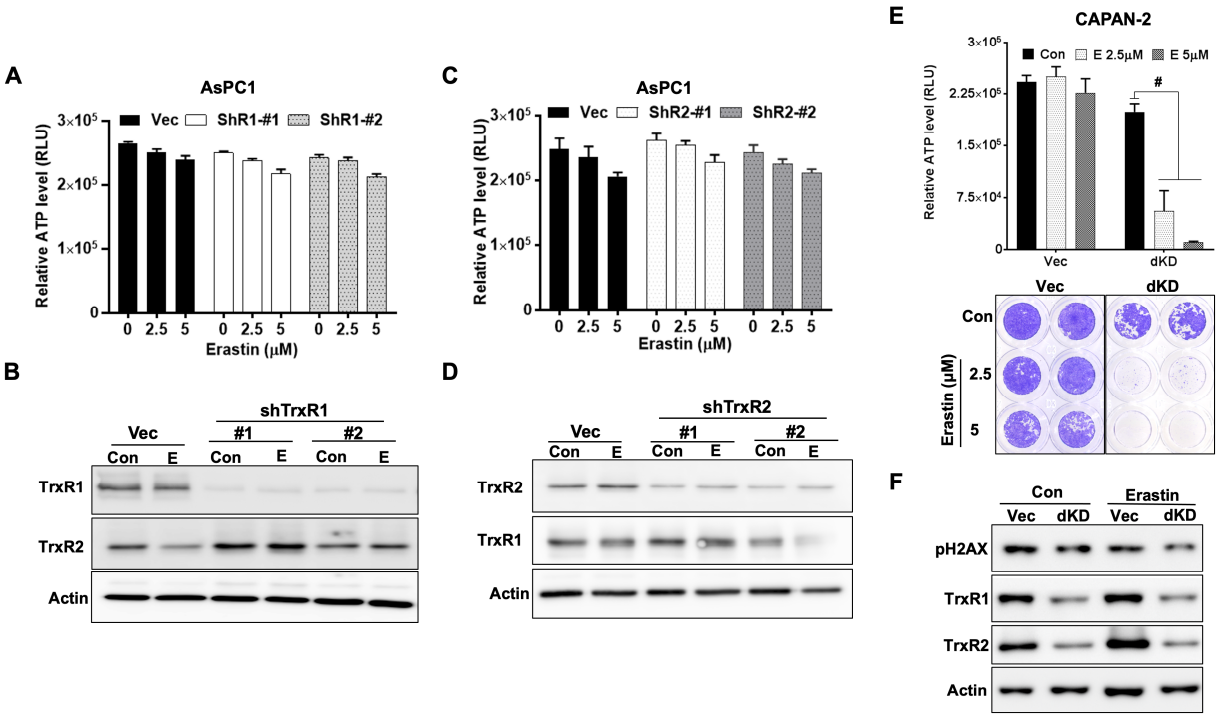


Figure 6. Suppression of TrxR expression sensitizes pancreatic tumor cells to erastin. (**A**). Relative viability of AsPC-1 vector control (Vec) and shTrxR1 (shR1) cells treated with control or erastin for 72 h ($n = 3$, $p > 0.05$). (**B**). Immunoblot analysis of TrxRs protein expression in AsPC-1 Vec and independent shTrxR1 clones after treatment with control or erastin (5 μM) for 72 h. (**C**). Relative viability of AsPC1 Vec and shTrxR2 (shR2) cells treated with control or erastin for 72 h ($n = 3$, $p > 0.05$). (**D**). Immunoblot analysis of TrxRs protein expression in AsPC1 Vec and shTrxR2 cells after treatment with control or erastin (5 μM) for 72 h. (**E**). Relative viability of Capan-2 Vec and double-knockdown (dKD; shTrxR1 + shTrxR2) cells, measured by CellTiter-Glo® assay and Crystal Violet staining, after treatment with control or erastin (2.5 or 5 μM) for 72 h ($n = 3$, # $p < 0.001$). (**F**). Immunoblot analysis of indicated protein expression in Vec control and dKD cells after treatment with either control or 5 μM erastin for 16 h.

To determine whether combined inhibition is required to overcome resistance, we generated a double knockdown (dKD) of both TrxR1 and TrxR2 (Figure 6F). Strikingly, dKD rendered erastin-resistant cells highly sensitive to erastin, producing robust cell death (Figure 6E).

Thioredoxin reductase activity and thioredoxin redox state were not directly measured in these experiments; therefore, we interpreted TrxR involvement based on functional perturbation using pharmacologic inhibition and dual TrxR1/TrxR2 suppression. Together, these findings demonstrate that epithelial-type PDAC cells rely on both TrxR1 and TrxR2 to maintain resistance to erastin-induced ferroptosis. Dual inhibition of cytosolic and mitochondrial thioredoxin pathways is therefore required to overcome this resistance and restore ferroptosis vulnerability.

3. Discussion

Ferroptosis has emerged as a metabolic vulnerability in multiple tumor types, including PDAC. The present study identifies two phenotypically distinct PDAC subgroups with differential dependence on cysteine and divergent susceptibility to ferroptosis, demonstrating that ferroptosis sensitivity is not uniformly distributed across pancreatic tumor cells. Our findings build on recent reports underscoring the metabolic heterogeneity of

PDAC and extend prior work by linking EMT state, selenium utilization, and thioredoxin reductase function to ferroptosis resistance [12,13,24,48,55].

We first show that mesenchymal-like PDAC cells exhibit pronounced cysteine dependence and rapid ferroptotic death upon system xc^- inhibition or direct GPX4 blockade, whereas epithelial-type cells remain largely resistant under the same conditions. These data support an emerging view that EMT status is associated with ferroptosis sensitivity, consistent with observations in breast cancer and other tumors [19,27,31]. Our transcriptomic clustering and GSEA analyses reinforce this association, showing that ferroptosis-sensitive PDAC cells are enriched mesenchymal gene signatures, while ferroptosis-resistant cells predominantly express epithelial markers. This aligns with recent PDAC-focused ferroptosis reviews suggesting rewiring of redox metabolism and lipid composition during EMT may dictate ferroptosis sensitivity [24,27,32]. However, our findings emphasize that EMT status functions primarily as a correlational biomarker rather than a direct mechanistic driver, as modulating Smad4 alone was insufficient to alter ferroptosis phenotypes. Direct manipulation of EMT inducers such as ZEB1, SNAIL, or TWIST, together with functional analysis of EMT-associated lipid remodeling pathways, will be required to determine whether EMT programs actively dictate ferroptosis susceptibility. At present, EMT status is best viewed as a phenotypic biomarker that distinguishes differences in ferroptosis sensitivity rather than serving as a direct mechanistic driver.

Because EMT and TGF-β signaling influence selenium metabolism and redox balance, Sepp1 emerged from our gene expression analysis as a candidate modulator. However, functional testing revealed that Sepp1 is not required for ferroptosis resistance, despite its differential expression between PDAC subtypes. This is an important clarification, as prior studies linked Sepp1 deficiency to increased ROS production and stem-like phenotypes [56], suggesting a potential regulatory role. Our results demonstrate that Sepp1 does not determine cysteine dependence, ferroptosis sensitivity, or erastin response in epithelial-type of PDAC cells, suggesting that selenium-mediated protection is mediated through other components of the antioxidant network. This conclusion is further supported by recent studies demonstrating that selenium availability alone does not determine GPX4 activity; instead, selenium is redistributed among selenoproteins in a cell state-dependent manner [41,42].

We next addressed how selenium supplementation robustly protects cells from ferroptosis. Although selenium increased GPX4 protein expression, intracellular GSH remained severely depleted under erastin plus selenium, rendering GPX4 catalytically inactive. This observation strongly argues that selenium may protect PDAC cells through GPX4-independent mechanisms as well, consistent with emerging reports showing that alternative selenoproteins, including PRDX6 and noncanonical selenium-utilization pathways, can modulate ferroptosis independently of GPX4 [26,33,41,42,58]. Notably, recent work demonstrated that PRDX6 functions as a selenium gatekeeper, determining whether selenium is allocated to GPX4 versus other selenoproteins, and thereby controlling ferroptosis sensitivity under cysteine stress [41,42]. Although we did not directly examine PRDX6 in this study, the selective preservation of thioredoxin reductase function under selenium treatment suggests that epithelial PDAC cells may prioritize selenium toward the thioredoxin axis rather than GPX4. This hypothesis is worth investigating in future.

Our pharmacologic and genetic data identify the thioredoxin system, specifically thioredoxin reductases TrxR1 and TrxR2, as the key selenium-dependent ferroptosis defense mechanism in these cells. TrxRs are selenoproteins whose activity can increase with selenium availability, and the Trx/TrxR axis operates parallel to the GPX4/GSH pathway to detoxify ROS [26,49,51]. Inhibition of TrxR activity using D9 or Auranofin abolished selenium-mediated protection and restored ferroptosis sensitivity, reactivating oxidative

stress signaling, DNA damage, and lipid peroxidation. These results are consistent with recent studies showing that TrxR1 inhibition sensitizes multiple cancer types to ferroptosis via GPX4-independent redox collapse [26,51]. Importantly, our identification of dual TrxR1/TrxR2 dependency highlights a cooperative cytosolic–mitochondrial redox axis, suggesting that epithelial-type PDAC cells rely on multi-compartment thioredoxin buffering to withstand cysteine deprivation. This is consistent with newly proposed models in which mitochondrial lipid peroxidation and mitochondrial–cytosolic ROS exchange act as amplifiers of ferroptotic stress [26]. Further biochemical assessment of TrxR enzymatic activity, thioredoxin redox state, and subcellular ROS distribution would offer a more comprehensive understanding of the underlying redox mechanisms.

Importantly, single knockdown of TrxR1 or TrxR2 alone did not restore ferroptosis sensitivity, revealing functional redundancy between the cytosolic and mitochondrial TrxR isoforms. Double knockdown (TrxR1/TrxR2) was required to induce ferroptotic death in response to erastin. Although we did not directly quantify TrxR activity or thioredoxin redox state and recognize that D9 lacks complete selectivity and may exert off target effects, the agreement between pharmacologic inhibition (D9 and auranofin) and dual TrxR1/TrxR2 suppression supports an on-target requirement for the thioredoxin system. This finding highlights that epithelial PDAC cells rely on both cytosolic and mitochondrial thioredoxin pathways to maintain redox homeostasis under cysteine-deprived conditions, underscoring the cooperative requirement for these enzymes in ferroptosis resistance. This redundancy mirrors patterns observed in other cancer contexts in which mitochondria-derived hydroperoxides act as initiating or amplifying signals for ferroptotic cell death, requiring suppression at both the mitochondrial and cytosolic levels to fully restore susceptibility [26,49].

From a translational standpoint, our work suggests that EMT markers and thioredoxin pathway components may serve as functional biomarkers to identify patients for ferroptosis-based therapies, complementing recent analyses of ferroptosis gene signatures in PDAC [15,28]. Combination strategies that co-target cysteine metabolism and thioredoxin reductases may help overcome ferroptosis resistance and exploit subtype-specific metabolic vulnerabilities [11]. Moreover, recent ferroptosis guidelines emphasize the need to therapeutically exploit cofactor limitations, such as GSH depletion and selenium competition, to force cells into redox collapse [16,48]. Our data indicate that selenium's protective capacity depends on preserving TrxR activity in addition to maintaining GPX4 expression, highlighting thioredoxin reductases as a rational therapeutic vulnerability in epithelial PDAC. However, our experiments in this study were conducted in vitro. Future studies extending these findings to three-dimensional culture systems, patient-derived organoids, and in vivo animal models will be necessary to validate the physiological relevance of the selenium–thioredoxin axis and to define its therapeutic potential in PDAC.

Overall, these data uncover a selenium–thioredoxin redox axis that contributes to ferroptosis resistance in epithelial PDAC cells (Figure 7) and provide a mechanistic framework for developing precision ferroptosis therapies tailored to PDAC subtype, EMT status, and antioxidant pathway usage. Future work integrating selenium-partitioning regulators such as PRDX6, EMT-linked lipidomic remodeling, and redox-cofactor dynamics will further clarify how subsets of PDAC cells sustain resistance to ferroptosis.

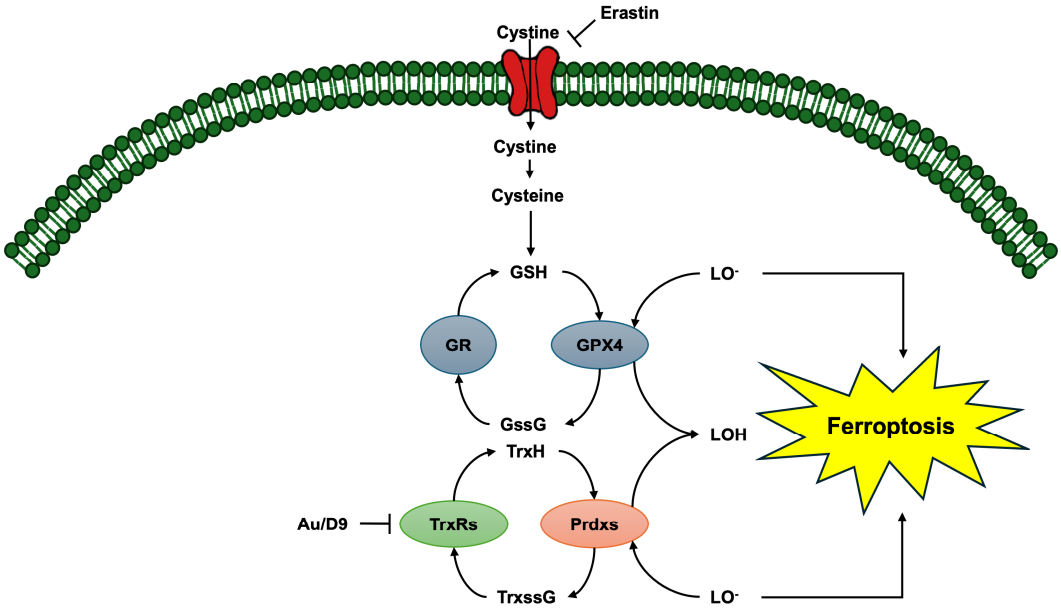


Figure 7. Schematic model illustrating the critical role of the thioredoxin system in regulating erastin-induced ferroptosis.

4. Materials and Methods

4.1. Cell Culture and Reagents

Pancreatic tumor cell lines and HEK293T cells were obtained from ATCC (Manassas, VA, USA) and cultured according to standard protocols in a humidified incubator (95% humidity, 5% CO_2, 37 °C). All cell lines were maintained in DMEM supplemented with 10% heat-inactivated fetal bovine serum (FBS) and 1% penicillin–streptomycin, unless otherwise specified. Cysteine-deficient medium was prepared according to a previously published protocol [19]. Death inhibitors Q-VD-OPH, Necrostatin-1, and Ferrostatin-1, as well as the ferroptosis inducer erastin, were purchased from Cayman Chemical (Ann Arbor, MI, USA). Sodium selenite (selenium source) was obtained from Sigma-Aldrich (St. Louis, MO, USA). Thioredoxin reductase inhibitors D9 and Auranofin were purchased from MedChem Express (South Brunswick, NJ, USA). All compounds were applied either individually or simultaneously as co-treatments, without any pretreatment. A complete list of antibodies (Cell Signaling Technologies, Danvers, MA, USA) used in this study is provided in Supplementary Table S1.

4.2. Lentiviral Cell Infection

Lentiviral particles were produced in HEK293T cells by transfecting lentiviral packaging plasmids together with the respective shRNA constructs using Lipofectamine 3000 (Thermo Fisher Scientific, Waltham, MA, USA). Viral supernatants were collected 48 h after transfection, clarified by centrifugation, and used immediately for infection or stored at −80 °C. Target cells were infected with viral supernatant for 48 h, followed by antibiotic selection with either puromycin or blasticidin (Cayman Chemical) to establish stable knockdown lines. shRNAs targeting Sepp1, TrxR1, and TrxR2 were obtained from Sigma-Aldrich, and the empty pLKO.1 vector served as the infection control.

4.3. Heatmap Cluster Analysis and Pathway Enrichment Analysis

Gene expression profiling data from six pancreatic cancer cell lines were retrieved from the GEO database (accession number GSE21654). Probe intensities were normalized using the Robust Multi-array Average (RMA) algorithm. Gene expression changes were

calculated as $\Delta\log_2$ (zero-transformed) values relative to the corresponding reference samples. Probe sets displaying at least a twofold change were selected for hierarchical clustering to visualize differential gene expression patterns across the cell lines. Pathway enrichment analysis was performed using Gene Set Enrichment Analysis (GSEA) with the G2 annotated gene sets and default settings, including 1000 permutations, to identify significantly enriched biological pathways.

4.4. RNA Extraction and Real-Time RT-PCR

Total RNA was isolated using the PureLink™ RNA Kit (Invitrogen, Carlsbad, CA, USA) according to the manufacturer's instructions. Two micrograms of RNA were reverse-transcribed into cDNA, and quantitative real-time PCR (qRT-PCR) was performed using SYBR Green PCR Master Mix (Applied Biosystems, Foster City, CA, USA). mRNA expression levels were normalized to ActB (β-actin) using the ΔΔCt method. All primer sequences used in this study are provided in Supplementary Table S2.

4.5. Immunoblotting Analysis

Cells were lysed in RIPA buffer (Sigma-Aldrich) supplemented with protease and phosphatase inhibitor cocktails (Thermo Fisher Scientific). Protein concentrations were quantified using the BCA assay, and equal amounts of total protein were resolved by SDS-PAGE and transferred to PVDF membranes. Immunoreactive bands were detected using the ECL Plus chemiluminescence system (GE Healthcare, Piscataway, NJ, USA) and visualized with the LAS-4000 imaging analyzer (GE Healthcare).

4.6. Cell Viability and Cytotoxicity

Cell viability was assessed either by measuring intracellular ATP levels using the CellTiter-Glo Assay Kit (Promega, Madison, WI, USA) or by Crystal Violet staining. Cells were seeded and treated in triplicate for all experiments. Cytotoxicity was evaluated using the CytoTox-Fluor Assay Kit (Promega), which quantifies protease activity released from damaged or membrane-compromised cells. Luminescence and fluorescence signals were recorded using a Synergy LX multimode plate reader (BioTek, Winooski, VM, USA).

4.7. Detection of Cellular Lipid Peroxidation, H_2O_2, and Glutathione

Lipid peroxidation was measured using the Image-iT™ Lipid Peroxidation Kit (Invitrogen). Cells were seeded in 96-well plates and treated in triplicate. After treatment, the kit reagent was added and incubated for 30 min, followed by replacement with Live Cell Imaging Solution (Thermo Fisher Scientific). Fluorescence was recorded at ~590 nm (oxidized, red) and ~510 nm (reduced, green) using a Synergy LX multimode reader (BioTek). The red/green ratio was calculated and normalized to total cellular protein or ATP content. In addition, fluorescent images were captured using the ZOE™ Fluorescent Cell Imager (Bio-Rad, Hercules, CA, USA).

Intracellular H_2O_2 levels were quantified using the ROS-Glo™ H_2O_2 Assay Kit (Promega), and glutathione (GSH) levels were measured using the GSH-Glo™ Glutathione Assay Kit (Promega) according to the manufacturer's instructions. Luminescence signals were collected using a Synergy LX multimode reader (BioTek) and normalized to total protein content.

4.8. Statistical Analysis

All experiments were performed with at least three biological replicates unless otherwise specified, and results were confirmed in a minimum of two independent experiments. Statistical significance between groups was assessed using unpaired two-tailed Student's *t*-tests, unless otherwise specified. All analyses were performed using GraphPad Prism

8.0, and p-values < 0.05 were considered statistically significant. Data are presented as mean ± standard deviation (SD) from at least three independent replicates.

Supplementary Materials: The following supporting information can be downloaded at: https://www.mdpi.com/article/10.3390/ijms27042062/s1.

Author Contributions: A.A. (Arslan Amer), M.I., A.A. (Aqsa Ahsan), A.A. (Alyssa Abbas) and T.A. contributed to methodology, investigation, validation, and data analysis; A.A. (Arslan Amer), M.I., A.A. (Aqsa Ahsan) and X.T. contributed to writing, reviewing, and editing of the manuscript; X.T. supervised the project and oversaw project administration and funding acquisition. All authors have read and agreed to the published version of the manuscript.

Funding: This research was partially supported by the National Institutes of Health (Grant #1R15CA246336-01 to X.T.) and by a Fulbright Fellowship awarded to A. Amer and A. Ahsan.

Institutional Review Board Statement: Not applicable.

Informed Consent Statement: Not applicable.

Data Availability Statement: The raw data supporting the conclusions of this article will be made available by the authors on request.

Conflicts of Interest: The authors have declared no conflict of interest for this study.

References

1. Siegel, R.L.; Giaquinto, A.N.; Jemal, A. Cancer statistics, 2024. *CA Cancer J. Clin.* **2024**, *74*, 12–49. [CrossRef]
2. Rahib, L.; Smith, B.D.; Aizenberg, R.; Rosenzweig, A.B.; Fleshman, J.M.; Matrisian, L.M. Projecting cancer incidence and deaths to 2030: The unexpected burden of thyroid, liver, and pancreas cancers in the United States. *Cancer Res.* **2014**, *74*, 2913–2921, Erratum in *Cancer Res.* **2014**, *74*, 4006. [CrossRef]
3. Conroy, T.; Hammel, P.; Hebbar, M.; Ben Abdelghani, M.; Wei, A.C.; Raoul, J.-L.; Choné, L.; Francois, E.; Artru, P.; Biagi, J.J.; et al. FOLFIRINOX or Gemcitabine as Adjuvant Therapy for Pancreatic Cancer. *N. Engl. J. Med.* **2018**, *379*, 2395–2406. [CrossRef]
4. McGuigan, A.; Kelly, P.; Turkington, R.C.; Jones, C.; Coleman, H.G.; McCain, R.S. Pancreatic cancer: A review of clinical diagnosis, epidemiology, treatment and outcomes. *World J. Gastroenterol.* **2018**, *24*, 4846–4861. [CrossRef]
5. Raphael, B.J.; Hruban, R.H.; Aguirre, A.J.; Moffitt, R.A.; Yeh, J.J.; Stewart, C.; Robertson, G.; Cherniack, A.D.; Gupta, M.; Getz, G.; et al. Integrated Genomic Characterization of Pancreatic Ductal Adenocarcinoma. *Cancer Cell* **2017**, *32*, 185–203.e13. [CrossRef] [PubMed]
6. Hanahan, D.; Weinberg, R.A. Hallmarks of cancer: The next generation. *Cell* **2011**, *144*, 646–674. [CrossRef]
7. Lunt, S.Y.; Vander Heiden, M.G. Aerobic glycolysis: Meeting the metabolic requirements of cell proliferation. *Annu. Rev. Cell Dev. Biol.* **2011**, *27*, 441–464. [CrossRef] [PubMed]
8. Moffitt, R.A.; Marayati, R.; Flate, E.L.; Volmar, K.E.; Loeza, S.G.; Hoadley, K.A.; Rashid, N.U.; Williams, L.A.; Eaton, S.C.; Chung, A.H.; et al. Virtual microdissection identifies distinct tumor- and stroma-specific subtypes of pancreatic ductal adenocarcinoma. *Nat. Genet.* **2015**, *47*, 1168–1178. [CrossRef] [PubMed]
9. Wu, H.; Fu, M.; Wu, M.; Cao, Z.; Zhang, Q.; Liu, Z. Emerging mechanisms and promising approaches in pancreatic cancer metabolism. *Cell Death Dis.* **2024**, *15*, 553. [CrossRef]
10. Yamamoto, K.; Iwadate, D.; Kato, H.; Nakai, Y.; Tateishi, K.; Fujishiro, M. Targeting the Metabolic Rewiring in Pancreatic Cancer and Its Tumor Microenvironment. *Cancers* **2022**, *14*, 4351. [CrossRef]
11. Lin, H.; Zhu, S.; Chen, Y.; Lu, J.; Xie, C.; Liao, C.; Huang, X.; Li, G.; Wu, Y.; Li, Z.; et al. Targeting cTRIP12 counteracts ferroptosis resistance and augments sensitivity to immunotherapy in pancreatic cancer. *Drug Resist. Updat.* **2025**, *81*, 101240. [CrossRef]
12. Lyu, H.; Kong, J.; Chen, J.; Zhang, R.; Xiao, S.; Guo, D.; Zhang, Q.; Chen, X.Z.; Tang, J.; Zhou, C. The Emerging Scenario of Ferroptosis in Pancreatic Cancer Tumorigenesis and Treatment. *Int. J. Mol. Sci.* **2024**, *25*, 13334. [CrossRef]
13. Yang, C.; Dong, Q.; Bao, H.; Ge, Y.; Xu, Z.; Li, J.; Jiang, X.; Xu, Y.; Zhong, X. Ferroptosis: New Strategies and Ideas for the Treatment of Pancreatic Ductal Adenocarcinoma. *Front. Biosci. (Landmark Ed.)* **2024**, *29*, 45. [CrossRef]
14. Dixon, S.J.; Lemberg, K.M.; Lamprecht, M.R.; Skouta, R.; Zaitsev, E.M.; Gleason, C.E.; Patel, D.N.; Bauer, A.J.; Cantley, A.M.; Yang, W.S.; et al. Ferroptosis: An iron-dependent form of nonapoptotic cell death. *Cell* **2012**, *149*, 1060–1072. [CrossRef]
15. Chen, Q.; Liu, F.; Zhang, Y.; Yan, L.; Wu, Y.; Xu, D.; Wu, P.; Yuan, H.; Jiang, K. Ferroptosis in cancer toward molecular insights and clinical translation in pancreatic cancer. *Mol. Cancer* 2026, *in press*. [CrossRef] [PubMed]

16. Li, Y.; Li, Z.; Li, Q.; Sun, D.; Ni, B.; Tan, M.; Shay, A.E.; Wang, M.; Meng, C.; Shen, G.; et al. Adaptation to cystine limitation stress confers a targetable lipid metabolism vulnerability in pancreatic ductal adenocarcinoma. *Nat. Commun.* **2025**, *17*, 1343. [CrossRef]
17. Badgley, M.A.; Kremer, D.M.; Maurer, H.C.; DelGiorno, K.E.; Lee, H.-J.; Purohit, V.; Sagalovskiy, I.R.; Ma, A.; Kapilian, J.; Firl, C.E. Cysteine depletion induces pancreatic tumor ferroptosis in mice. *Science* **2020**, *368*, 85–89. [CrossRef]
18. Gai, C.; Liu, C.; Wu, X.; Yu, M.; Zheng, J.; Zhang, W.; Lv, S.; Li, W. MT1DP loaded by folate-modified liposomes sensitizes erastin-induced ferroptosis via regulating miR-365a-3p/NRF2 axis in non-small cell lung cancer cells. *Cell Death Dis.* **2020**, *11*, 751. [CrossRef] [PubMed]
19. Tang, X.; Ding, C.K.; Wu, J.; Sjol, J.; Wardell, S.; Spasojevic, I.; George, D.; McDonnell, D.P.; Hsu, D.S.; Chang, J.T.; et al. Cystine addiction of triple-negative breast cancer associated with EMT augmented death signaling. *Oncogene* **2017**, *36*, 4235–4242. Erratum in *Oncogene* **2017**, *36*, 4379. https://doi.org/10.1038/onc.2017.192. [CrossRef]
20. Lo, M.; Ling, V.; Low, C.; Wang, Y.Z.; Gout, P.W. Potential use of the anti-inflammatory drug, sulfasalazine, for targeted therapy of pancreatic cancer. *Curr. Oncol.* **2010**, *17*, 9–16. [CrossRef] [PubMed]
21. Timmerman, L.A.; Holton, T.; Yuneva, M.; Louie, R.J.; Padró, M.; Daemen, A.; Hu, M.; Chan, D.A.; Ethier, S.P.; van 't Veer, L.J.; et al. Glutamine sensitivity analysis identifies the xCT antiporter as a common triple-negative breast tumor therapeutic target. *Cancer Cell* **2013**, *24*, 450–465. [CrossRef]
22. Graczyk-Jarzynka, A.; Zagozdzon, R.; Muchowicz, A.; Siernicka, M.; Juszczynski, P.; Firczuk, M. New insights into redox homeostasis as a therapeutic target in B-cell malignancies. *Curr. Opin. Hematol.* **2017**, *24*, 393–401. [CrossRef] [PubMed]
23. Cramer, S.L.; Saha, A.; Liu, J.; Tadi, S.; Tiziani, S.; Yan, W.; Triplett, K.; Lamb, C.; Alters, S.E.; Rowlinson, S.; et al. Systemic depletion of L-cyst(e)ine with cyst(e)inase increases reactive oxygen species and suppresses tumor growth. *Nat. Med.* **2017**, *23*, 120–127. [CrossRef]
24. Zhou, Q.; Meng, Y.; Li, D.; Yao, L.; Le, J.; Liu, Y.; Sun, Y.; Zeng, F.; Chen, X.; Deng, G. Ferroptosis in cancer: From molecular mechanisms to therapeutic strategies. *Signal Transduct. Target. Ther.* **2024**, *9*, 55. [CrossRef] [PubMed]
25. Yapici, F.I.; Bebber, C.M.; von Karstedt, S. A guide to ferroptosis in cancer. *Mol. Oncol.* **2024**, *18*, 1378–1396. [CrossRef] [PubMed]
26. Ding, X.; Cui, L.; Mi, Y.; Hu, J.; Cai, Z.; Tang, Q.; Yang, L.; Yang, Z.; Wang, Q.; Li, H.; et al. Ferroptosis in cancer: Revealing the multifaceted functions of mitochondria. *Cell Mol. Life Sci.* **2025**, *82*, 277. [CrossRef]
27. Ebrahimi, N.; Adelian, S.; Shakerian, S.; Afshinpour, M.; Chaleshtori, S.R.; Rostami, N.; Rezaei-Tazangi, F.; Beiranvand, S.; Hamblin, M.R.; Aref, A.R. Crosstalk between ferroptosis and the epithelial-mesenchymal transition: Implications for inflammation and cancer therapy. *Cytokine Growth Factor Rev.* **2022**, *64*, 33–45. [CrossRef]
28. Chung, T.T.; Piao, Z.; Lee, S.J. Identification of ferroptosis-related signature predicting prognosis and therapeutic responses in pancreatic cancer. *Sci. Rep.* **2025**, *15*, 75. [CrossRef]
29. Dreyer, S.B.; Upstill-Goddard, R.; Legrini, A.; Biankin, A.V.; Glasgow Precision Oncology, L.; Jamieson, N.B.; Chang, D.K.; Australian Pancreatic Genome, I.; Jamieson, N.B.; Chang, D.K. Genomic and Molecular Analyses Identify Molecular Subtypes of Pancreatic Cancer Recurrence. *Gastroenterology* **2022**, *162*, 320–324.e4. [CrossRef]
30. Bailey, P.; Chang, D.K.; Nones, K.; Johns, A.L.; Patch, A.M.; Gingras, M.C.; Miller, D.K.; Christ, A.N.; Bruxner, T.J.; Quinn, M.C.; et al. Genomic analyses identify molecular subtypes of pancreatic cancer. *Nature* **2016**, *531*, 47–52. [CrossRef]
31. Schwab, A.; Rao, Z.; Zhang, J.; Gollowitzer, A.; Siebenkas, K.; Bindel, N.; D'Avanzo, E.; van Roey, R.; Hajjaj, Y.; Ozel, E.; et al. Zeb1 mediates EMT/plasticity-associated ferroptosis sensitivity in cancer cells by regulating lipogenic enzyme expression and phospholipid composition. *Nat. Cell Biol.* **2024**, *26*, 1470–1481. [CrossRef]
32. Zhang, H.; Chen, N.; Ding, C.; Zhang, H.; Liu, D.; Liu, S. Ferroptosis and EMT resistance in cancer: A comprehensive review of the interplay. *Front. Oncol.* **2024**, *14*, 1344290. [CrossRef]
33. Tschuck, J.; Skafar, V.; Friedmann Angeli, J.P.; Hadian, K. The metabolic code of ferroptosis: Nutritional regulators of cell death. *Trends Biochem. Sci.* **2025**, *50*, 663–676. [CrossRef]
34. Kryukov, G.V.; Castellano, S.; Novoselov, S.V.; Lobanov, A.V.; Zehtab, O.; Guigó, R.; Gladyshev, V.N. Characterization of mammalian selenoproteomes. *Science* **2003**, *300*, 1439–1443. [CrossRef]
35. Hatfield, D.L.; Schweizer, U.; Tsuji, P.A.; Gladyshev, V.N. *Selenium Its Molecular Biology and Role in Human Health*; Springer International Publishing, A.G.: Berlin/Heidelberg, Germany, 2018.
36. Conrad, M.; Proneth, B. Selenium: Tracing Another Essential Element of Ferroptotic Cell Death. *Cell Chem. Biol.* **2020**, *27*, 409–419. [CrossRef]
37. Short, S.P.; Williams, C.S. Selenoproteins in Tumorigenesis and Cancer Progression. *Adv. Cancer Res.* **2017**, *136*, 49–83. [PubMed]
38. Friedmann Angeli, J.P.; Schneider, M.; Proneth, B.; Tyurina, Y.Y.; Tyurin, V.A.; Hammond, V.J.; Herbach, N.; Aichler, M.; Walch, A.; Eggenhofer, E. Inactivation of the ferroptosis regulator Gpx4 triggers acute renal failure in mice. *Nat. Cell Biol.* **2014**, *16*, 1180–1191. [CrossRef] [PubMed]
39. Yang, W.S.; Stockwell, B.R. Synthetic lethal screening identifies compounds activating iron-dependent, nonapoptotic cell death in oncogenic-RAS-harboring cancer cells. *Chem. Biol.* **2008**, *15*, 234–245. [CrossRef] [PubMed]

40. Burk, R.F.; Hill, K.E.; Motley, A.K.; Winfrey, V.P.; Kurokawa, S.; Mitchell, S.L.; Zhang, W. Selenoprotein P and apolipoprotein E receptor-2 interact at the blood-brain barrier and also within the brain to maintain an essential selenium pool that protects against neurodegeneration. *FASEB J.* **2014**, *28*, 3579–3588. [CrossRef]
41. Fujita, H.; Tanaka, Y.K.; Ogata, S.; Suzuki, N.; Kuno, S.; Barayeu, U.; Akaike, T.; Ogra, Y.; Iwai, K. PRDX6 augments selenium utilization to limit iron toxicity and ferroptosis. *Nat. Struct. Mol. Biol.* **2024**, *31*, 1277–1285. [CrossRef]
42. Ito, J.; Nakamura, T.; Toyama, T.; Chen, D.; Berndt, C.; Poschmann, G.; Mourao, A.S.D.; Doll, S.; Suzuki, M.; Zhang, W.; et al. PRDX6 dictates ferroptosis sensitivity by directing cellular selenium utilization. *Mol. Cell* **2024**, *84*, 4629–4644.e9. [CrossRef]
43. Gencheva, R.; Cheng, Q.; Arner, E.S. Thioredoxin reductase selenoproteins from different organisms as potential drug targets for treatment of human diseases. *Free. Radic. Biol. Med.* **2022**, *190*, 320–338. [CrossRef]
44. Zhang, J.; Chen, Y.; Fang, J. Targeting thioredoxin reductase by micheliolide contributes to radiosensitizing and inducing apoptosis of HeLa cells. *Free. Radic. Biol. Med.* **2022**, *186*, 99–109. [CrossRef] [PubMed]
45. Hintze, K.J.; Wald, K.A.; Zeng, H.; Jeffery, E.H.; Finley, J.W. Thioredoxin reductase in human hepatoma cells is transcriptionally regulated by sulforaphane and other electrophiles via an antioxidant response element. *J. Nutr.* **2003**, *133*, 2721–2727. [CrossRef]
46. Zhang, J.; Li, X.; Zhao, Z.; Cai, W.; Fang, J. Thioredoxin signaling pathways in cancer. *Antioxid. Redox Signal.* **2023**, *38*, 403–424. [CrossRef] [PubMed]
47. Patwardhan, R.S.; Sharma, D.; Sandur, S.K. Thioredoxin reductase: An emerging pharmacologic target for radiosensitization of cancer. *Transl. Oncol.* **2022**, *17*, 101341. [CrossRef] [PubMed]
48. Dai, E.; Chen, X.; Linkermann, A.; Jiang, X.; Kang, R.; Kagan, V.E.; Bayir, H.; Yang, W.S.; Garcia-Saez, A.J.; Ioannou, M.S.; et al. A guideline on the molecular ecosystem regulating ferroptosis. *Nat. Cell Biol.* **2024**, *26*, 1447–1457. [CrossRef]
49. Wang, W.; Mou, Y.; Lu, D.; Xu, S. Involvement of the thioredoxin system in multiple diseases: A focus on mechanisms of action in autophagy and ferroptosis (Review). *Mol. Med. Rep.* **2026**, *33*, 27. [CrossRef]
50. Zhang, Y.; Sun, S.; Xu, W.; Yang, R.; Yang, Y.; Guo, J.; Ma, K.; Xu, J. Thioredoxin reductase 1 inhibitor shikonin promotes cell necroptosis via SecTRAPs generation and oxygen-coupled redox cycling. *Free. Radic. Biol. Med.* **2022**, *180*, 52–62. [CrossRef]
51. Hsieh, M.S.; Ling, H.H.; Setiawan, S.A.; Hardianti, M.S.; Fong, I.H.; Yeh, C.T.; Chen, J.H. Therapeutic targeting of thioredoxin reductase 1 causes ferroptosis while potentiating anti-PD-1 efficacy in head and neck cancer. *Chem. Biol. Interact.* **2024**, *395*, 111004. [CrossRef]
52. Alothaim, T.; Charbonneau, M.; Tang, X. HDAC6 inhibitors sensitize non-mesenchymal triple-negative breast cancer cells to cysteine deprivation. *Sci. Rep.* **2021**, *11*, 10956. [CrossRef]
53. Dolma, S.; Lessnick, S.L.; Hahn, W.C.; Stockwell, B.R. Identification of genotype-selective antitumor agents using synthetic lethal chemical screening in engineered human tumor cells. *Cancer Cell* **2003**, *3*, 285–296. [CrossRef] [PubMed]
54. Ahmed, S.; Bradshaw, A.D.; Gera, S.; Dewan, M.Z.; Xu, R. The TGF-β/Smad4 Signaling Pathway in Pancreatic Carcinogenesis and Its Clinical Significance. *J. Clin. Med.* **2017**, *6*, 5. [CrossRef] [PubMed]
55. Collisson, E.A.; Sadanandam, A.; Olson, P.; Gibb, W.J.; Truitt, M.; Gu, S.; Cooc, J.; Weinkle, J.; Kim, G.E.; Jakkula, L.; et al. Subtypes of pancreatic ductal adenocarcinoma and their differing responses to therapy. *Nat. Med.* **2011**, *17*, 500–503. [CrossRef] [PubMed]
56. Barrett, C.W.; Reddy, V.K.; Short, S.P.; Motley, A.K.; Lintel, M.K.; Bradley, A.M.; Freeman, T.; Vallance, J.; Ning, W.; Parang, B. Selenoprotein P influences colitis-induced tumorigenesis by mediating stemness and oxidative damage. *J. Clin. Investig.* **2015**, *125*, 2646–2660. [CrossRef]
57. Benhar, M.; Shytaj, I.L.; Stamler, J.S.; Savarino, A. Dual targeting of the thioredoxin and glutathione systems in cancer and HIV. *J. Clin. Investig.* **2016**, *126*, 1630–1639. [CrossRef]
58. Lee, N.; Park, S.J.; Lange, M.; Tseyang, T.; Doshi, M.B.; Kim, T.Y.; Song, Y.; Kim, D.I.; Greer, P.L.; Olzmann, J.A.; et al. Selenium reduction of ubiquinone via SQOR suppresses ferroptosis. *Nat. Metab.* **2024**, *6*, 343–358. [CrossRef]

Disclaimer/Publisher's Note: The statements, opinions and data contained in all publications are solely those of the individual author(s) and contributor(s) and not of MDPI and/or the editor(s). MDPI and/or the editor(s) disclaim responsibility for any injury to people or property resulting from any ideas, methods, instructions or products referred to in the content.